ISSN 1392 - 1207. MECHANIKA. 2007. Nr.4(66)

Numerical stress analysis of granular material

R. Balevičius*, D. Markauskas**
**Vilnius Gediminas Technical University, Saulėtekio al. 11, 10223 Vilnius, Lithuania,*
E-mail: Robertas.Balevicius@st.vtu.lt
***Vilnius Gediminas Technical University, Saulėtekio al. 11, 10223 Vilnius, Lithuania, E-mail: dm@fm.vtu.lt*

1. Introduction

The knowledge about granular materials is rather limited compared to the respective information on the solids, while a unified theory encompassing all granular material phenomena has not been created yet [1].

Despite the fact that granular material is the discontinuous media its behavior is commonly described by the continuum approach. Consequently, the definition of stresses in granular material is a controversial topic of mechanics [2, 3]. In particular, some researchers (e.g. [4]) claim that the stress tensor is asymmetric and the coupled stresses responding to the material instabilities, such as shear bending, exist. Others (e.g. [5]) affirm that stress asymmetry is not bound or can be negligible in practical predictions.

The simplified continuum models are used to predict the pressure fields, especially those acting on the walls but they have serious drawbacks in evaluating the effects occurring on the particle level. Furthermore, the experimental stress investigations within the granular material are also complicated, requiring non-invasive and precise contact force measurements [6, 7]. An alternative is to perform DEM-based [8] simulations and then average the particle contact forces and their contact locations over the particular volumes. Such numerical studies based on the linkage of microscopic variables in discrete concept to the macroscopic variables in continuum approach can be found in e.g. [3], [9, 10].

In the current research, the numerical stress analysis of granular material, based on discrete particle model involving laws of single particle contact mechanics and the effects of friction as well as viscous damping forces is performed. Verification of the obtained results and their compatibility with well-known continuum-based indications are also demonstrated.

2. Theoretical background

Let us consider the volume V of a granular material filled with N number of spheres. Some of them can be subjected to external forces applied from the exterior, while internal forces acting on the particles are represented by the particle contact forces. From the experimental investigations (e.g. [6, 7]), it is well known that the force amplitude fluctuates from contact to contact. From theoretical point of view, it is also well known (e.g. [5]) that the macroscopic mean stress tensor can generally be derived from the microscopic quantities of discrete particle, such as the contact force distribution and the contact location, as their complex homogenization over the volume V

$$\boldsymbol{\sigma}_{ij} = \frac{1}{V}\sum_{c\in V} F_i^c l_j^c \tag{1}$$

where $\boldsymbol{F}^c$ and $\boldsymbol{l}^c$ are contact force and contact position vector at the contact c while i (j) denotes the ith (jth) component of these vectors over the range i,j=1, 2, 3 or $i,j\equiv$x, y, z.

In general, the symmetrical stress tensor σ_{ij} defines the three-dimensional state of stresses which act on three mutual perpendicular planes at a given point of granular material.

Now let us consider the assembly of granules bound by rigid walls into a cuboid shape. The particles contacting with the walls cause wall reaction forces that can be treated as external actions on the granular assembly. The assembly of particles subjected to the external forces is in equilibrium, when each particle subjected to the action of internal (contact) forces is in equilibrium. Therefore, the stresses, acting on cuboid faces, can be simply found if the corresponding particle-wall reaction force vectors $\boldsymbol{R}^{c_w}$ at the contact c_w are known. They are as follows

$$\boldsymbol{\sigma}_{ij} = \frac{\sum_{c_w} R_{ij}^{c_w}}{A_i} \tag{2}$$

where A_i is the ith face area of the cuboid.

Since Eq. (1) substantially produces averaged stresses in the centre of the volume, averaged reaction forces must also be used in Eq. (2). In these formulations, the first subscript refers to the face of cuboid on which the stress acts and the second subscript refers to the direction in which the associated force acts.

Thus, the stresses resulted from their homogenization in the given volume, according to Eq. (1) and those induced by wall reaction forces, according to Eq. (2), will be verified below.

3. Numerical analysis

The current numerical analysis is intended to: analyze stress distribution within granular material caused mainly by the granular material weight and friction; explore inaccuracies that can arise from the numerical implementation of Eq. (1) or the continuum representation by *a priori* chosen amount of the discrete particles; evaluate the stresses obtained by Eq. (1) comparing them with those obtained by Eq. (2). The circumstances of the comparison are attributed to frictionless and frictional granular material.

3.1. The technique used

Stress analysis of granular material involving different analysis techniques could be found in literature. For instance, Bardet [2] analytically investigated the reason for stress asymmetry in double and multiple layers, while Lagrange's multiplier method, mainly based on statistical physics, was implemented by Evesque [11] in modeling the densifying of spherical granules. Nevertheless, the discrete element method, introduced by Cundall and Strack [8] has been recognized as a more powerful and universal tool for such analysis. Therefore, the DEM technique based on [12-14] was implemented in the current simulation and is briefly described below.

Let us consider the kinematics and contact geometry of two spherical particles plotted in Fig. 1.

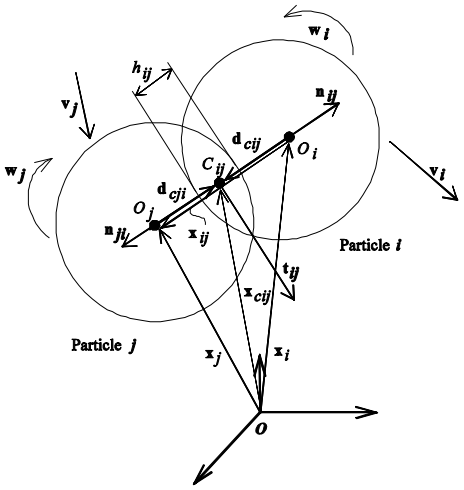

Fig. 1 Contact geometry of the particles

Two particles in contact, *i* and *j*, are defined by their positions $\boldsymbol{x}_i$ and $\boldsymbol{x}_j$, representing the locations of the centres of gravity O_i and O_j (Fig. 1). Position of the particles is time-dependent. The particles are subjected to the translational velocities $\boldsymbol{v}_i$ and $\boldsymbol{v}_j$, as well as the rotation velocities $\boldsymbol{w}_i$ and $\boldsymbol{w}_j$.

In terms of DEM, the particles are treated as individual objects with their own dynamical parameters (position, velocity, etc.). Therefore, the dynamics of each particle can be defined by forces and torques acting on the particle and described by a system of dynamical equations within Newton's laws

$$m_i \frac{d^2 \boldsymbol{x}_i}{dt^2} = \sum_{j=1, j\neq i} \boldsymbol{F}_{ij} + m_i \boldsymbol{g} \tag{3}$$

$$I_i \frac{d^2 \boldsymbol{\theta}_i}{dt^2} = \sum_{j=1, j\neq i} \boldsymbol{d}_{cij} \times \boldsymbol{F}_{ij} \tag{4}$$

where $\boldsymbol{x}_i$, $\boldsymbol{\theta}_i$ are position vectors of the of the centre of gravity and orientation of the particle (Fig. 1), m_i is the mass of the particle *i* (i = 1, …, *N*), I_i is inertia moment of the particle, $\boldsymbol{F}_{ij}$ is inter-particle or particle-wall contact forces acting on the contact centre point C_{ij} (Fig. 1), $\boldsymbol{d}_{cij}$ is the vector specifying the position of the contact point C_{ij} with respect to the centers of contacting particles (Fig. 1), $\boldsymbol{g}$ is the vector of gravity acceleration, while *t* is the time considered.

Contact deformation of the particle *i* with respect to another particle *j* is approximated by representative overlap area in the vicinity of contact centre point C_{ij}. Hence, the resulting contact force $\boldsymbol{F}_{ij}$ arising from a visco-elastic collision between particles *i* and *j* and acting on this point is expressed in terms of the normal and the tangential components

$$\boldsymbol{F}_{ij} = \boldsymbol{F}^{e}_{n,ij} + \boldsymbol{F}^{v}_{n,ij} - \boldsymbol{t}_{ij}\, min\left(\left|\boldsymbol{F}^{st}_{t,ij}\right|, \left|\boldsymbol{F}^{dyn}_{t,ij}\right|\right) \tag{5}$$

where $\boldsymbol{F}^{e}_{n,ij} = \frac{2}{3}\cdot\frac{E}{\left(1-\nu^2\right)} R_{ij}^{2-\alpha} h_{ij}^{\alpha} \boldsymbol{n}_{ij}$ and $\boldsymbol{F}^{v}_{n,ij} = -\gamma_n m_{ij} \boldsymbol{v}_{n,ij}$ are the vectors of elastic and viscous damping forces normal to the contact surface; α is the power coefficient (for Hooke's law, α = 1); E and ν are the elastic modulus and Poisson's ratio of particle material, h_{ij} is the overlap (Fig. 1), R_{ij} and m_{ij} are the normalized radius and normalized mass, $\boldsymbol{n}_{ij}$ is the unit vector normal to the contact surface (Fig. 1); $\boldsymbol{F}^{st}_{t,ij} = -\frac{8}{3}\cdot\frac{G\sqrt{R_{ij} h_{ij}}}{(2-\nu)} \int \boldsymbol{v}_{t,ij}(t)dt - \gamma_t m_{ij} \boldsymbol{v}_{t,ij}$ as well as $\boldsymbol{F}^{dyn}_{t,ij} = -\mu\left|\boldsymbol{F}^{e}_{n,ij} + \boldsymbol{F}^{v}_{n,ij}\right| \boldsymbol{t}_{ij}$ are the vectors of static and dynamic friction forces acting in tangential to the contact surface direction, $\boldsymbol{t}_{ij}$ is the unit vector of tangential direction depending on tangential velocity (Fig. 1), $\boldsymbol{v}_{n,ij}$ and $\boldsymbol{v}_{t,ij}$ are the normal and tangential components of contact velocities depending on $\boldsymbol{v}_i$ and $\boldsymbol{v}_j$, as well as $\boldsymbol{w}_i$ and $\boldsymbol{w}_j$, γ_n and γ_t are the viscous damping coefficients in normal and tangential directions.

A detailed description of the above force models can be found in [12, 14].

Relating the stress tensor from Eq. (1) with Eq. (5) and relying on the similarity of the contact geometry outlined in (

Fig. 1), the equality of $\boldsymbol{F}^{c} \equiv \boldsymbol{F}_{ij}$ and $\boldsymbol{l}^{c} \equiv \boldsymbol{d}_{cij}$ are used in the current analysis.

The time-dependent contact forces $\boldsymbol{F}_{ij}$ are computed at each time step by applying contact searching algorithm described in [13]. Linkage of these forces with the particle dynamical parameters is performed by resolving Eqs. (3) and (4) by using *5th – order Gear's predictor-corrector* scheme [12, 14].

3.2. Description of the tests

The tests performed involve numerical simulation of granular material behavior for frictionless and frictional particles. The material is considered as an assembly of N = 1980 particles. The values of the particle radii R_i, ranging from 0.03 to 0.035 m, are generated by using uniform distribution. Total mass M of the material is fixed to be the same for frictionless and frictional particles and is equal to M = 143.7 kg. The main data on the visco-elastic granules are given in Table.

The granular assembly is subjected to two-stage compaction in the defined size of the box. The first part involves particle compaction due to their free fall, while the second stage comprises particle compaction by the moving wall.

Table

Basic data on granules

Quantity	Symbol	Value
Density, kg/m^3	ρ	500
Poisson's ratio	ν	0.30
Elasticity modulus, Pa	E	$0.3 \cdot 10^6$
Shear modulus, Pa	G	$0.11 \cdot 10^6$
Friction coefficient	μ	0; 0.3
Normal viscous damping coefficient, 1/s	γ_n	60.0
Tangential viscous damping coefficient, 1/s	γ_t	10.0

The creation of granular assembly starts from the particles falling due to the fixed gravity acceleration in the box (Fig. 2).

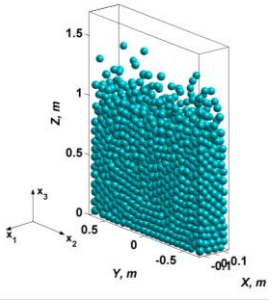

Fig. 2 Behavior of the particles under the compaction caused by gravity (μ=0)

For this purpose, the space above the box was divided into cubic cells as an orthogonal and uniform 3D grid of 0.1 m size. Initially, at time t = 0, the particles were embedded into the centers of the cells and were free of contact. In order to mix up the particles during their settling the initial particle velocities are artificially imposed. The fields of particle velocities were defined randomly by uniform distribution and variation of their magnitude over the range of 0-0.3 m/s. The frictionless particles behavior at the time instance, t=1 s, the size of the box and the system of global coordinates are shown in Fig. 2.

The end of the first stage of compaction is assumed to be a quasistatic state of particles which underwent negligible small velocities. The occurrence of a quasistatic mode was controlled by the system's kinetic energy.

In order to slightly consolidate the settled material and to control numerically the changes in the volume of particles assembly, the particles compaction by the moving wall was adopted in the second stage. Thus, the theoretically assumed time instance of the quasistatic stage is fixed as the time of the second stage beginning. Consequently, a new time scale referred to as the initial time t = 0 was employed and all dynamical parameters of the particles obtained at the quasistatic mode were assumed to be the initial conditions. The top wall motion was induced by imposing vertical velocity equal to $v_{bc,z}$=-0.01 m/s. The duration of the second stage was assumed to be 1s, which lead to vertical deformation of the assembly equal to -9.2 ‰ and -8.6 ‰ for frictionless and frictional material, respectively.

3.3. Results and discussion

Let us firstly consider the results obtained for frictionless particles. This assembly of particles, for which the stress computations will be performed later is depicted in Fig. 3. The obtained structure of granules was captured at the end of the first compaction stage, while the color-bar depicted shows the inter-particle contact forces, $\sum_{i \neq j} \left| \boldsymbol{F}_{ij} \right|$. These forces will be used to calculate stress tensor (1).

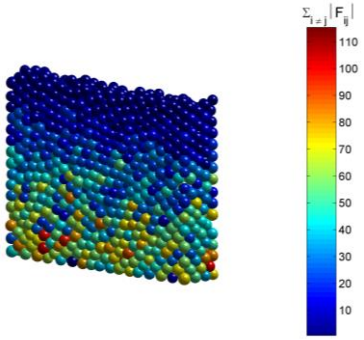

Fig. 3 The assembly of particles (μ=0) and the particle forces (measured in N)

In Fig. 3, the formation of material layers having different inter-particle contact force values is shown. The magnitudes of these forces at the top surface are much lower compared to those at the bottom, since these forces are caused by the weight of the granules. In the upper layers, these forces are distributed more uniformly, while the layers above the bottom wall are characterized by less-uniformly distributed contact forces.

The plots of vertical force equilibrium during the second stage of compaction (i.e. compaction by the moving wall) are shown in Fig. 4.

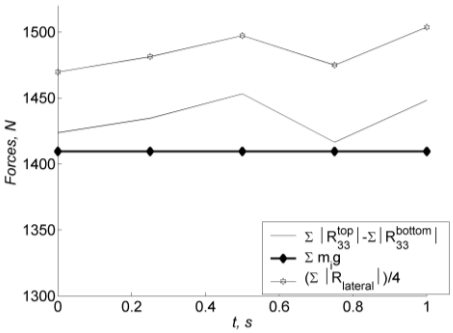

Fig. 4 Forces vs time (μ=0)

In the graphs of Fig. 4, equilibrium between the reactions of the top and bottom walls (R_{33}^{top} and R_{33}^{bottom}, respectively) and the force induced by the particles weight can be treated as satisfying. A relatively low artificial damping, (error, ranging from 0.4% to 3%), indicates that the particles assembly subjected to external (wall reaction) forces and internal (contact) forces is in equilibrium. Moreover, the visible time-fluctuation in reaction forces indicates that the assembly of frictionless particles is sufficiently sensitive to external action produced by the moving wall. On the other hand, the time fluctuation of wall reaction forces is related to the wave of inter-particle contact force propagation within the material.

The obtained horizontal reaction averaged over all vertical walls ($1/4 \sum \left| R_{lateral} \right|$) is quite close to the vertical

reaction produced by horizontal walls, since the average area of vertical walls is two times greater than the area of the bottom in the current simulation (Fig. 4).

At time instance t=1s, the average stress tensor (in Pa) computed by Eq. (1) in the whole volume of the assembly shown in Fig. 3 is as follows

$$\boldsymbol{\sigma}_{ij} = \begin{bmatrix} -1663.1 & 3.5 & 16.6 \\ 3.5 & -1550.2 & 4.3 \\ 16.6 & 4.3 & -1637.0 \end{bmatrix}$$

As it can be seen, the values of shear stresses are sufficiently low, but not equal to zero, while three normal stresses are approximately equal, showing the fact that the assembly of frictionless particles is subjected to near-hydrostatic pressure. Negative sign of normal stress denotes the material compression.

The obtained nonzero shear stresses are mainly attributed to a relatively small number of particles used in simulation and produce a certain friction effect resulted from the particle coordination peculiarities. It should be expected, that, with the increase of the particles number the difference between the components of normal stresses could be smaller, covering zero shear.

The graphs comparing normal stresses computed by Eq. (1) and Eq. (2) are plotted in Fig. 5.

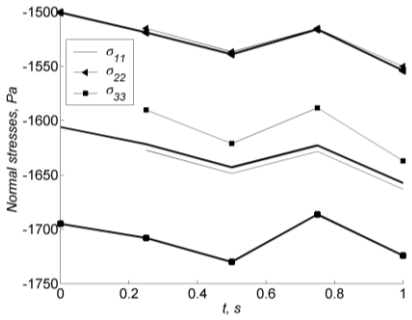

Fig. 5 Normal stresses vs time in frictionless granular material. Thin lines – Eq. (1), bold lines - Eq. (2)

As it is shown in Fig. 5, there is a good coincidence between normal stresses homogenized in the given volume by Eq. (1) and those produced by the averaged wall reactions according to Eq. (2). The difference in stress σ_{33}, reaching up to 6%, is attributed to the above mentioned friction effect.

Let us consider the results obtained for granular material which has the friction, μ=0.3. The obtained structure of the assembly is shown in Fig. 6. By comparing the particle forces depicted in Fig. 3 and Fig. 6, it can clearly be indicated that frictional material has non-uniform force distribution in the assembly. This means that some of the particles are subjected to higher contact forces than their neighbours. The observed bulk volume of the frictional assembly is greater than the volume of frictionless material. The linked stress arches that form between the particles lead to increasing in the bulk volume and thus increase the overall porosity of the assembly.

The plots of vertical forces for frictional material are shown in Fig. 7.

These graphs show the well-known fact that frictional material transfers weight toward vertical walls via friction forces. The difference between vertical reactions of the top and bottom wall versus material weight indicates that the part of about 10% of the material weight is transmitted to the vertical walls by its shear forces. This portion is quite small due to a sufficiently small size of the model used. It can also be seen, that there is no fluctuation of the reaction forces in time, what shows that the frictional particles are not sensitive (opposite to frictionless particles) to the given external action produced by the moving wall.

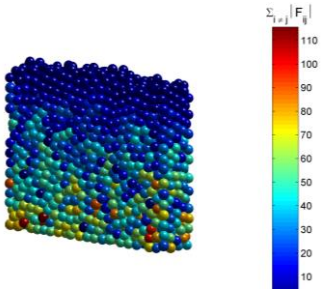

Fig. 6 Assembly of particles (μ=0.3) and the particle forces (measured in N)

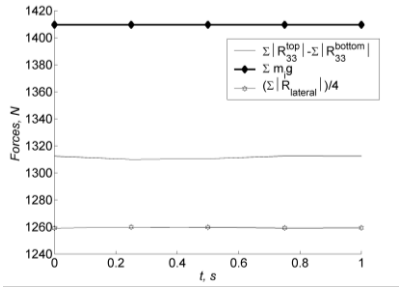

Fig. 7 Forces vs time (μ=0.3)

At the time instance t=1 s, the average stress tensor (in Pa) homogenized by Eq. (1) in the volume of frictional particles' assembly shown in

Fig. 6 is as follows

$$\boldsymbol{\sigma}_{ij} = \begin{bmatrix} -1299.80 & 0.423 & -0.413 \\ 0.221 & -1284.66 & -21.43 \\ -0.422 & -22.51 & -1516.53 \end{bmatrix}$$

Since the stress tensor (1) is symmetric, any computed asymmetry in $\boldsymbol{\sigma}_{ij}$ should be interpreted as an inaccurate calculation or the lack of static equilibrium. The obtained stress values indicate that the symmetry in stress is effectively satisfied. The relatively small inconsistence is found for stresses σ_{12} and σ_{21}. This could also be attributed to the assembly thinness as was pointed out in [2]. In addition, the condition $|\sigma_{33}| > |\sigma_{11}| > |\sigma_{22}|$ suggests that active stress state occurs after the first stage of compaction [15].

The graphs comparing normal stresses computed by Eqs. (1) and (2) (bold lines) in frictional granular media are plotted in Fig. 8.

Fig. 8 shows good matching of normal stresses homogenized in the given volume by Eq. (1) and those produced by the averaged walls reaction for frictional particles. The difference up to 3% is mainly referred to the stress σ_{33}.

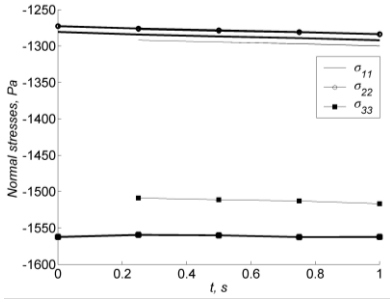

Fig. 8 Normal stresses vs time in frictional material. Thin lines – Eq. (1), bold lines - Eq. (2)

It is very difficult to make accurate stress measurements within the bulk mass of the material by experiments. Nevertheless, there are continuum-based indications about the distribution of stresses within granular material. Verifying these assumptions, let us now consider the distribution of stresses within granular material obtained numerically.

For the stress derivation within the granular material, the whole volume was divided into representative spheres, while microscopic quantities of the particle within these spheres were homogenized by using Eq. (1). The volume of the material within a given sphere was defined by excluding particle overlaps, while the volume of the representative sphere adjacent to the wall was also determined, relying on the sphere-wall intersection geometry. The computed stress tensor components were then displayed on a spatial grid. This was made by using a three-dimensional cubic spline interpolation/extrapolation procedure, allowing computing the values of spatial stress function on the intermediate and out-of-the range points of the grid. The obtained distribution of normal stress σ_{33} within the frictional granular assembly is presented in Fig. 9. The midsection stress was captured at the end of the first stage of compaction.

As shown in Fig. 9, the normal stress σ_{33} increases with the increase of the material depth, *z*, since it is caused by the material weight. Moreover, at any vertical cross-section the computed $\sigma_{33}(z)$ is nonlinearly dependent on material depth *z* indicating that particles friction forces transmit the material weight towards vertical walls. The quantitative illustration of this, considering wall reaction forces can also be found (Fig. 7).

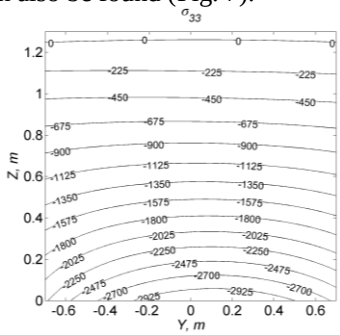

Fig. 9 Distribution of σ_{33} in frictional granular material (μ=0.3)

The distribution of normal stresses (Fig. 9) has a convex shape with peak values at the centre and lower values at the wall planes due to the increase of shear stress toward the walls. In particular, the obtained convex shape of σ_{33} is well-coincident with the asymptotic stress distribution found by Drescher [16] by using the method of characteristics in the analysis of hopper wall pressure.

The eigenvalues, as well as eigenvectors, of stress tensor (1) were also analyzed. The eigenvalues represent principal stresses, while eigenvectors denote orientations of the planes, on which the principal stresses act (see sketch on Fig. 10). The trajectories of the principal stress σ_1 represented as eigenvectors n_1 are plotted at the end of the first compaction stage in Fig. 10.

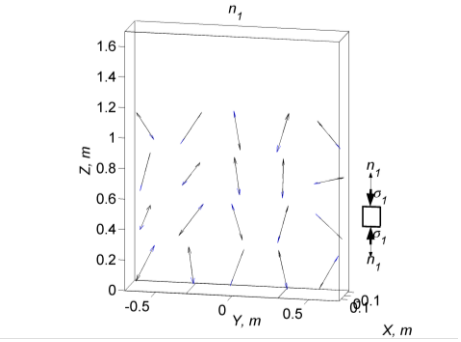

Fig. 10 Trajectories of the principal stress σ_1 (μ=0.3)

From the continuum analysis [16], it follows that for the corresponding active stress state the trajectories of σ_1 are approximately vertical with a slight bending towards the walls due to shear. The obtained numerical results shown in Fig. 10 are effectively consistent with this indication.

4. Concluding remarks

It is very difficult to make experimentally accurate stress measurements within the bulk mass of material. Consequently, a discrete particle model based on inter-particle contact forces with laws of classical Newton's mechanics was applied to stress numerical analysis in granular material. The macroscopic stress tensor was homogenized by Eq. (1), taking into account microscopic quantities of particles, and then comparing it with the normal stresses produced by the averaged wall reactions by Eq. (2). The accuracy of these results was satisfactory. After verification, the obtained stresses were examined in terms of well-established assumptions of the continuum mechanics.

In particular, the contribution of friction forces (produced by a discrete particle model) on bulk material weight transmitted toward vertical walls was revealed by the wall's reaction forces, the distribution of normal stresses within the material as well as by the respective values of the mean stress tensor (1). The obtained convex shape of vertical normal stress distribution is well-coincident with the asymptotic stress character prevailing for an active stress state.

The computed mean stress tensor (1) for an assembly of granules satisfied sufficiently the continuum-based conditions on shear stress symmetry, while the determined trajectories of principal stress were effectively consistent with the indications of the continuum-based approach.

The obtained nonzero shear stresses for friction-

less material were mainly attributed to a relatively small number of the particles used, producing certain heterogeneity of material and resulting in a portion of friction. It should be also noted that discrete particle micromechanical properties contribute the stress fields that would be more precise with increasing number of the particles in the model.

The results obtained may contribute to better understanding of microscopic–macroscopic behavior of granular material.

References

1. **De Gennes, P.G.** Reflections on the mechanics of granular matter.-Physica A, 1998, 261, p.267-293.
2. **Bardet, J. P., Vardoulakis, I.** The asymmetry of stress in granular media.-Int. J. Solids Struct., 2001, v.38, No2, p.353-367.
3. **Luding, S.** From DEM simulations towards a continuum theory of granular material.-Powders & Grains -Lisse: Swets&Zeitlinger, 2001, p.141-148.
4. **Chang, C.S., Ma, L.** A micromechanical-based micropolar theory for deformation of granular solids.-Int. J. Solids Struct., 1991, v.28, No1, p.67-86.
5. **Christoffersen, J., Mehrabadi, M., Nemat-Nasser, S.** A micro-mechanical description of granular material behavior.-J. Appl. Mech., 1981, v.48, No2, p.339-344.
6. **Howell, D.W., Behringer, R.P., Veje, C.T.** Fluctuations in granular media.-Chaos, 1999, v.9, No3, p.559-572.
7. **Drescher, A., de Josselin de Jong, G.** Photo-elastic verification of a mechanical model for the flow of granular material.-J. Mech. Phys. Solids, 1972, v.20, No5, p.337-351.
8. **Cundall, P.A., Strack, O.D.L.** A discrete numerical model for granular assemblies.-Geotechnique, 1979, v.29, No1, p.47-65.
9. **Zhu, H.P., Yu, A.B.** Steady-state granular flow in 3D cylindrical hopper with flat bottom: macroscopic analysis.-Granular Matter, 2005, v.7, No2-3, p.97-107.
10. **Zhu, H.P., Yu, A.B.** Averaging method of granular materials-Phys. Rev. E, 2002, v.66, No2, p.021302-1–021302-15.
11. **Evesque, P.** Modeling the micro-macro passage in the quasi-statics regime of granular matter.-Powders & Grains -Lisse: Swets&Zeitlinger, 2001, p.153-156.
12. **Balevičius, R., Džiugys, A., Kačianauskas, R.** Discrete element method and its application to the analysis of penetration into granular media.-J. of Civil Engineering and Management, 2004, v.10, No1, p.3-14.
13. **Balevičius, R., Kačianauskas, R., Džiugys, A., Maknickas, A., Vislavičius, K.** Investigation of performance of programming approaches and languages used for numerical simulation of granular material by the discrete element method.-Computer Physics Communications, 2006, v.175, No6, p.404-415.
14. **Džiugys, A., Navakas, R., Šlančiauskas, A., Stravinskas, G., Kačianauskas, R.** Numerical simulation of mixing and segregation of granular material. -Mechanika, 2005, Nr.3(53), p.52-56.
15. **Nedderman, R. M.** Statics and Kinematics of Granular Materials.-New York: Cambridge University Press, 1992.-352p.
16. **Drescher, A.** Analytical Methods in Bin-load Analysis. -New York: Elsevier, 1991.-255p.

R. Balevičius, D. Markauskas

SKAITINIS GRANULIUOTOS MEDŽIAGOS ĮTEMPIŲ TYRIMAS

R e z i u m ė

Tiesiogiai išmatuoti granuliuotos medžiagos įtempius yra labai keblu. Todėl straipsnyje atliktas skaitinis šių įtempių modeliavimas įvertinant diskrečias daleles veikiančias jėgas. Pateikta gautų rezultatų verifikacija ir jų suderinamumas su žinomais kontinuumo mechanikos teiginiais.

R. Balevičius, D. Markauskas

NUMERICAL STRESS ANALYSIS OF GRANULAR MATERIAL

S u m m a r y

From the experimental point of view, it is very difficult to obtain accurate stress measurements within the bulk of granular material. The numerical stress analysis based on the forces acting on the discrete particle was performed. Verification of the obtained results and their compatibility with well-known continuum-based indications were demonstrated.

Р. Балявичюс, Д. Маркаускас

ЧИСЛЕННЫЙ АНАЛИЗ НАПРЯЖЕНИЙ В ГРАНУЛИРОВАННОМ МАТЕРИАЛЕ

Р е з ю м е

Измерение напряжений, действующих в гранулированном материале, экспериментальным путем всегда сопровождается большими трудностями. Поэтому в данной статье произведен их численный анализ на основе сил, действующих непосредственно на частицы материала. Дана проверка и совместимость полученных результатов с известными предпосылками механики сплошной среды.

Received May 25, 2007

DOI: 10.5755/j02.mech.14926